Influence of Reduced Winter Land–Sea Contrast on the Midlatitude Atmospheric Circulation

Alice Portal, Claudia Pasquero, Fabio D'andrea, Paolo Davini, Mostafa Hamouda, Gwendal Rivière

Influence of Reduced Winter Land–Sea Contrast on the Midlatitude Atmospheric Circulation

ALICE PORTAL,[a,b] CLAUDIA PASQUERO,[a,c] FABIO D'ANDREA,[b] PAOLO DAVINI,[c] MOSTAFA E. HAMOUDA,[d,e] AND GWENDAL RIVIÈRE[b]

[a] *Department of Earth and Environmental Sciences, Università di Milano-Bicocca, Milan, Italy*
[b] *Laboratoire de Météorologie Dynamique/IPSL, École Normale Supérieure, PSL Research University, Sorbonne Université, École Polytechnique, IP Paris, CNRS, Paris, France*
[c] *Consiglio Nazionale delle Ricerche, Istituto di Scienze dell'Atmosfera e del Clima (CNR-ISAC), Torino, Italy*
[d] *Astronomy and Meteorology Department, Faculty of Science, Cairo University, Cairo, Egypt*
[e] *Institute for Atmospheric and Environmental Sciences, Goethe University Frankfurt, Frankfurt am Main, Germany*

(Manuscript received 30 November 2021, in final form 21 May 2022)

ABSTRACT: Even though winter land–sea thermal contrast (LSC) is expected to undergo a strong weakening in the future warmer climate, its effects have been poorly investigated. Here we run a set of idealized winter simulations featuring reduced LSC in the Northern Hemisphere (NH) extratropics, or in individual extratropical sectors of the NH (Atlantic and Pacific), using an intermediate-complexity atmospheric general circulation model. Reduced LSC is obtained by imposing a warming of surface land temperatures in East Asia and North America. For similar warming intensities over the two regions, the response of the model to East Asia forcing is significantly stronger and dominates the response to the sum of the two forcing patterns. We find that the LSC reduction causes a weakening and poleward shift of the midlatitude jet streams, and a strong interference with zonal wavenumbers 1 and 2. In particular, East Asian warming reduces the amplitude of waves 1 and 2, producing a strengthening of the stratospheric vortex, while a weaker vortex due to a moderate amplification of wave 1 is detected when warming North America. Eventually, stratospheric signals propagate downward in the troposphere affecting the midlatitude winter NH even remotely from the forcing. In this work we pinpoint some mechanisms by which weakened winter LSC influences the NH extratropical circulation: the results may become useful to interpret the response to long-term projections displaying reduced LSC along with other climate change forcing patterns.

KEYWORDS: Atmospheric circulation; Planetary waves; Stratospheric circulation

1. Introduction

In the NH the winter thermal contrast between the cold continents and the relatively warmer oceans determines a consistent part of the diabatic heating pattern in the atmosphere (Smagorinsky 1953; Held 1983). This is of fundamental importance for the dynamics of the midlatitude atmosphere and, along with orography and tropical forcing, sets the shape of planetary waves throughout the troposphere (Held 1983; Held and Ting 1990; Held et al. 2002; Garfinkel et al. 2020). At synoptic frequencies, the strong thermal gradients between land and sea located at the eastern coasts of Asia and North America are a prominent source of baroclinicity and trigger the eastward-extending storm tracks feeding the jet streams across the Pacific and Atlantic basins (Hoskins and Valdes 1990; Brayshaw et al. 2009). At longer time scales the thermal-equilibration theory introduced by Charney and DeVore (1979) posits that the global-scale wavelike thermal structure generated by the asymmetric surface-temperature pattern induces a succession of equilibrated and forced regimes, where the midlatitude circulation resonates with the temperature structure or else is predominantly zonal (Marshall and So 1990; Mitchell and Derome 1983).

Among the features of long-term climate change projections, the most relevant in the middle and high latitudes are the Arctic amplification (AA) (Serreze and Barry 2011; Previdi et al. 2021) and a variation in the thermal land–sea contrast (LSC), which is expected to decrease in winter and increase in summer due to the faster warming of land surface compared to ocean surface (Sutton et al. 2007; Wallace and Joshi 2018; He et al. 2018). A number of studies address the impact of LSC changes on regional atmospheric dynamics, such as on tropical monsoons (Shaw and Voigt 2015; Zhuang et al. 2022), temperature variability (de Vries et al. 2012; Gregory and Mitchell 1995), and tropospheric circulation (Kamae et al. 2014; Day and Hodges 2018). Despite the rich literature assessing the importance of extratropical LSC for the midlatitude dynamics (e.g., Smagorinsky 1953; Held 1983; Valdes and Hoskins 1989; Held and Ting 1990; Held et al. 2002), limited attention is given to the influence of LSC on the future large-scale atmospheric circulation. The predicted variation in extratropical LSC is similar, in order of magnitude, to the AA (IPCC 2021), which, conversely, has been extensively studied for its links with the midlatitude circulation

Denotes content that is immediately available upon publication as open access.

Supplemental information related to this paper is available at the Journals Online website: https://doi.org/10.1175/JCLI-D-21-0941.s1.

Corresponding author: Alice Portal, a.portal@campus.unimib.it

DOI: 10.1175/JCLI-D-21-0941.1

[e.g., Cohen et al. (2020), Blackport and Screen (2020), and Labe et al. (2020), just to cite some of the most recent articles].

Midlatitude LSC is also known to play a role in the interannual-to-interdecadal atmospheric variability. He et al. (2014, 2018) find an impact of winter LSC on atmospheric circulation and atmospheric blocking using reanalysis and models. Molteni et al. (2011) use a different approach to investigate the role of the thermal contrast in forcing interdecadal variations in the northern annular mode (NAM) during the second half of the twentieth century. By running idealized experiments with an intermediate-complexity atmospheric model, they evidence the effects of a cold-ocean/warm-land pattern on the winter planetary-scale variability.

Here we use a similar procedure and the same model as Molteni et al. (2011) to study the large-scale tropospheric and stratospheric response to reduced winter midlatitude LSC, with a large-scale analysis covering frequencies from the stationary to the synoptic. In long-term climate projections a different warming of the Pacific and Atlantic Oceans is foreseen for the NH midlatitudes due to the so-called North Atlantic warming hole (i.e., a deficit in the North Atlantic warming rate) (Drijfhout et al. 2012). Such an asymmetry in the ocean surface warming implies a substantially weaker LSC at the eastern coast of North America compared with the East Asian one in the future climate. For this reason, and because the interannual evolution of Atlantic and Pacific LSC appears to be independent [the correlation coefficient between $\mathrm{LSC}_{\mathrm{Atl}}(t)$ and $\mathrm{LSC}_{\mathrm{Pac}}(t)$ is 0.07 using the yearly January–February time series from 1979 to 2020; see section 2 for the definition of $\mathrm{LSC}_{\mathrm{Pac,Atl}}$], we investigate the circulation response to reduced LSC over each basin independently. The individual basin approach is reminiscent of analyses of the atmospheric response to individual topographic structures, such as the Rockies or the Tibetan Plateau (Held et al. 2002, and references therein). The results of this work may be valuable for the interpretation of long-term climate change scenarios and for determining the role of LSC in the extratropical interannual variability.

The paper is organized as in the following. Section 2 provides a description of the model and of the set of sensitivity experiments, as well as a definition for Atlantic and Pacific LSC and of the main diagnostics; in section 3 we present the responses to different patterns of reduced LSC; in section 4 we summarize and discuss the main findings.

2. Methods

a. Model

We use an eight-level atmospheric general circulation model (AGCM) developed at the International Centre for Theoretical Physics (ICTP), known as SPEEDY (for Simplified Parameterization, Primitive Equation Dynamics). The model is spectral on the sphere, with triangular truncation at total wavenumber 30 (T30) and with an associated Gaussian grid of 96 × 48 points. Despite the low horizontal and vertical resolution, SPEEDY displays an adequate performance for the analysis of large-scale features of the climate system (Kucharski et al. 2013). While Molteni (2003) and Kucharski et al. (2006) provide a comprehensive description of the model and its climatology, in appendix A we supply a focus on the model stratosphere and in appendix B we report the details of the land surface temperature (LST) and sea ice temperature (SIT) schemes, including how the latter interacts with the sea surface temperature (SST). The schemes are switched on or off depending on the target of each simulation.

b. Experiments

We first perform an ensemble of ten 30-yr simulations with realistic SST and sea ice cover (SIC) conditions and with an active land surface temperature scheme and inactive sea ice temperature scheme.[1] The ensemble-mean monthly-averaged LST from this set of simulations, hereafter referred to as $\mathrm{LST}_{\mathrm{mod}}(m)$, with m indicating the month, is used to compute the forcing for a set of perpetual-winter simulations. The perpetual-winter integrations have LST fixed to the prescribed values, and SST set to the 1979–2008 HadISST climatology, with only its SIT component free to evolve.[2] The procedure for the construction of the perpetual-winter runs is similar to that in Molteni et al. (2011) and is described in the following.

(i) *Control*: two perpetual-winter control simulations (hereafter CONTROL), one for January and one for February, are run separately for 400 months with fixed SST, SIC and LST—the first two being the monthly HadISST climatologies, the latter being $\mathrm{LST}_{\mathrm{mod}}$. The CONTROL surface temperature is shown in Fig. 1a.

(ii) *Reduced land–sea contrast*: two perpetual-winter experiments, one for January and one for February, for each different forcing (hereafter TOTAL, ASIA, and NAMERICA) are run for 400 months with fixed LST, SST, and SIC. Whereas SST and SIC are as in the CONTROL, the LST for TOTAL forcing is constrained to a weighted mean between the January/February and the April $\mathrm{LST}_{\mathrm{mod}}$ (see appendix C for details on the computation). The forcing patterns are constructed in order to obtain similar intensities of the zonally integrated temperature anomaly and of LSC reduction over the two continents (see Fig. 1b for the TOTAL forcing, and Fig. 1c for the zonal-mean forcing considering solely East Asia or North America). Individual continent patterns are selected from the TOTAL forcing to run the experiments ASIA and NAMERICA.

When compared to Molteni et al. (2011), our experiments differ for two main reasons. First, a regional difference is applied in the forcing (details in appendix C) in order to obtain anomalies of similar intensity over the Pacific and Atlantic

[1] Each of the 10 ensemble members is forced by observed SST and by climatological SIC from the 1979–2008 monthly fields of HadISST reanalysis (see Rayner et al. 2003), with different initial conditions taken from the 1 January fields of a simulation constrained by climatological SST and SIC.

[2] The difference in average SIT between the forcing and control experiments is found to be negligible with respect to the amplitude of the LST forcing, and hence is not examined in section 3.

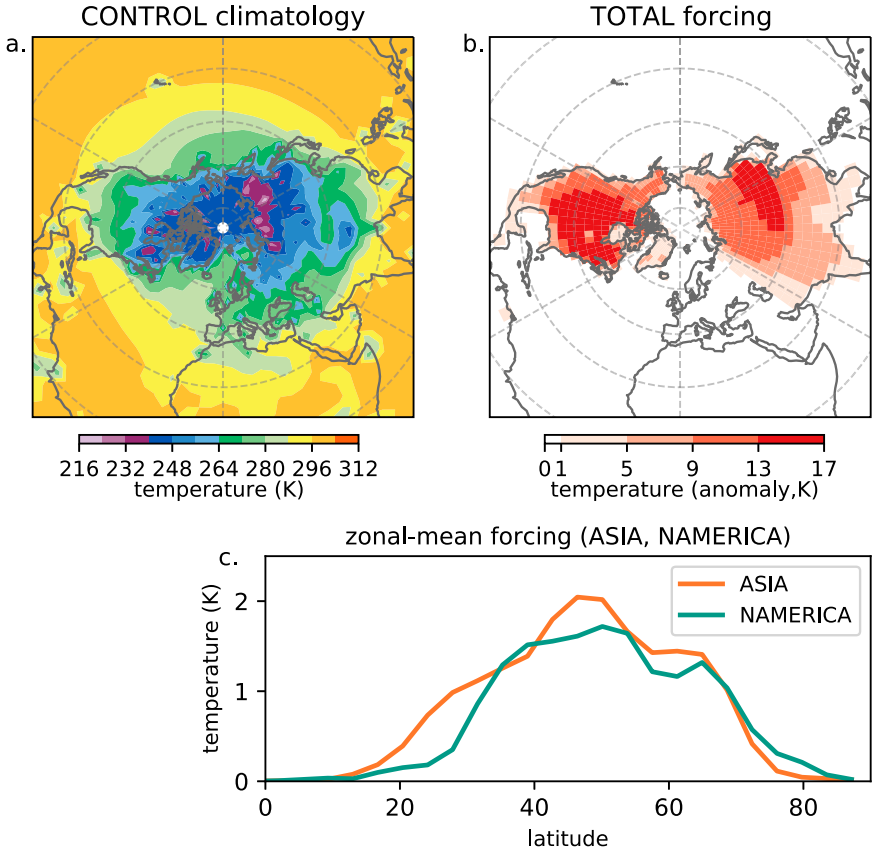

FIG. 1. (a) Surface temperature in CONTROL and (b) TOTAL forcing anomaly, averaged over January and February; (c) zonal-mean anomaly for individual-continent forcing—ASIA and NAMERICA—weighted by the cosine of latitude.

sectors; second, SST (apart from the SIT component) is kept as in the CONTROL so as not to influence the meridional temperature gradients over the midlatitude oceans. This means that the reduced-LSC experiments are subject to a net heating with respect to the CONTROL.

c. *Thermal land–sea contrast*

We define LSC over the extratropical Atlantic and Pacific sectors as the skin temperature difference between two boxes placed west and east of the western coastline (Fig. 2). Note that the forcing is applied in terms of LST, while the LSC is computed on the basis of skin temperature averages; the difference between the two variables is illustrated in appendix B. The values of LSC_{Atl} and LSC_{Pac} for the perpetual winter simulations are shown in Table 1, where they are compared to recent LSC (1979–2008 climatology from ECMWF ERA5; Hersbach et al. 2020) and to LSC in 2200–2300 climate change projections [mean over models CCSM4, CNRM-CM5, GISS-E2-R, and MPI-ESM-LR participating in the CMIP5 extended concentration pathways (RCP8.5); Taylor et al. 2012]. While in the CONTROL and TOTAL simulations and in the reanalysis (first three columns of Table 1) the values of LSC_{Atl} and LSC_{Pac} are of comparable amplitude, the long-term projections show a thermal contrast that is much larger over the western Pacific than over the western Atlantic (fourth column of Table 1). This is an effect of the slower warming predicted for the subpolar North Atlantic (North Atlantic warming hole) in response to the prospected change in the North Atlantic circulation (Keil et al. 2020; Rahmstorf et al. 2015), which, combined with the high warming rate of the North American continent, is expected to cause a strong reduction of the contrast between the cold winter continent and the relatively warmer ocean. A reduction in both Pacific and Atlantic LSC is already seen in observations; for example, a linear regression on ERA5 data shows a weakening of both LSC_{Pac} and LSC_{Atl} by 1.2 K (±1.0 K) between 1979 and 2020 (not shown).

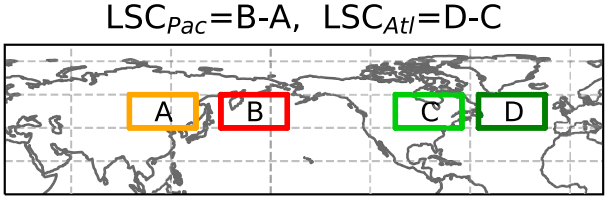

FIG. 2. Longitude–latitude boxes used to compute LSC_{Pac}(B − A) and LSC_{Atl}(D − C). The boxes are between latitudes 40° and 60°N and are 40° longitude wide (box A: 95°–135°E, box B: 150°–190°E, box C: 65°–105°W, box D: 15°–55°W).

TABLE 1. Atlantic and Pacific LSC in the CONTROL simulations and in the TOTAL experiments, in the 1979–2008 ERA5 climatology and in the RCP8.5 CMIP5 long-term projections for 2200–2300 (with the differences "TOT − CTRL" and "CMIP5 − ERA5" in square brackets and the standard deviation for ERA5 in parentheses). For experiments ASIA and NAMERICA the LSC is reduced only over one basin, the Pacific or Atlantic, respectively.

			ERA5	CMIP5–RCP8.5
	CTRL	TOTAL	1979–2008	2200–2300
LSC_{Atl}	22.4 K	13.9 [−8.5] K	23.3 (±1.8) K	11.1 [−12.2] K
LSC_{Pac}	21.6 K	12.8 [−8.8] K	21.7 (±1.9) K	16.6 [−5.1] K

d. Diagnostics

Daily model output is averaged over the January and February runs, excluding a spinup period of 165 days for each run. Here we introduce some daily diagnostics, useful for the analyses presented in section 3. First, the vertical component of the Eliassen–Palm flux is used to estimate the vertical propagation of planetary waves

$$\mathrm{EPf}_z \equiv a\cos(\phi)\,\frac{f}{\partial\overline{\theta_{\mathrm{cl}}}/\partial p}\,\overline{v^*T^*}, \tag{1}$$

where a is the radius of Earth, f is the Coriolis parameter dependent on latitude, $\overline{\theta_{\mathrm{cl}}}$ is the climatological zonal-mean potential temperature, and $\overline{v^*T^*}$ is the meridional eddy heat flux, with an overbar ($\bar{\cdot}$) denoting the zonal mean and an asterisk (*) the deviation from the zonal mean (eddy component). Similarly, the 200-hPa v^*T^* evidences the longitudinal features of the vertical wave propagation in the lower stratosphere.

A measure for baroclinicity is provided by the maximum Eady growth rate, as in the expression by Hoskins and Valdes (1990) comprising the module of the vertical derivative of the horizontal wind velocity $\mathbf{u}$ (not only the zonal component)

$$\sigma_{\mathrm{BI}} \equiv 0.31 f \left|\frac{\partial \mathbf{u}}{\partial z}\right| \mathcal{N}^{-1}, \tag{2}$$

with $\mathcal{N} \equiv \sqrt{(g/\theta)(d\theta/dz)}$ being the Brunt–Väisälä frequency (θ is the potential temperature, and g Earth's gravitational acceleration).

The high-frequency (HF) components of the geopotential height, wind, and potential temperature fields are selected using a 2–6-day Fourier bandpass filter in order to represent the high-frequency geopotential height variance (i.e., the storm track) and the eddy total energy flux (TEF; Drouard et al. 2015). The latter is used to estimate the downstream propagation of eddy total energy and is defined as

$$\mathrm{TEF} \equiv \mathbf{u}\cdot(\mathrm{EKE}+\mathrm{EAPE}) + \mathbf{u}_a^{\mathrm{HF}} Z^{\mathrm{HF}}, \quad \mathbf{u}_a \equiv \mathbf{u} - \frac{g\mathbf{k}}{f}\times\nabla Z, \tag{3}$$

with contributions from the advective flux of eddy kinetic energy (EKE) $\equiv (\mathbf{u}^{\mathrm{HF}})^2/2$, from eddy available potential energy (EAPE) $\equiv (h^2/s^2)(\theta^{\mathrm{HF}})^2/2$, and from the ageostrophic geopotential flux, described in terms of Z (geopotential height) and $\mathbf{u}_a$ (ageostrophic horizontal wind). The EAPE parameters $s^2 = -h\partial\theta_{\mathrm{cl}}/\partial p$ and $h = (R/p)(p/p_s)^{R/C_p}$ depend on pressure (R is the gas constant, p_s is 1000 hPa, and C_p is the specific heat of the air at constant pressure).

3. Results and discussion

a. Stationary waves

The stationary response of the model to the three configurations of surface forcing described in section 2 (TOTAL, ASIA, NAMERICA) is depicted in Fig. 3. The simulations with the TOTAL forcing are characterized by negative mean sea level pressure (MSLP) anomalies extending up to 60°N over North America and Asia and by a weakening of the Aleutian and Icelandic low pressure systems (Fig. 3a). The attenuation of the low pressure systems is linked to the decrease of the diabatic heating from the oceanic western boundary currents (surface heat flux in Fig. S1) and to the weakening of the midlatitude jets in Fig. 3j (Wang and Ting 1999; Held et al. 2002; Chang 2009; Kaspi and Schneider 2011). In the midtroposphere we find a general increase of the geopotential height in the middle and high latitudes, peaking downstream of the forcing, over the adjacent midlatitude basins (Fig. 3d). The surface pressure low to the east of the warming and the downstream high in geopotential height are found also in individual ASIA and NAMERICA experiments (Figs. 3b,e and 3c,f); both features are expected in correspondence of low-level heating anomalies in the midlatitudes (Kushnir et al. 2002). Moreover, the stationary eddy component (deviation from the zonal mean) of the geopotential height is strongly reduced (Fig. 3g), with a weakening of the cyclonic structure over Asia/Pacific and of the anticyclonic eddy over western North America. The pattern is reminiscent of the "thermal" stationary wave in Fig. 6.22 of Held (1983).

The resemblance of experiments TOTAL and ASIA (cf. Figs. 3a,d,g,j and 3b,e,h,k) proves that the global signal in TOTAL is dominated by the changes in Pacific LSC, and in particular that the Siberian surface pressure high is of great relevance in setting the shape of stationary planetary waves (Cohen et al. 2001). In fact, the widespread anomalies in experiment ASIA tend to reduce the stationary planetary waves in the midtroposphere, including the orographic wave over North America [cf. the eddy geopotential height in Fig. 3h to the response to Rocky Mountain topography in Fig. 6.9 of Held (1983)]. This last effect is linked to the weakening of the low-level Pacific jet impinging on the Rockies (Held and Ting 1990; discussed in more detail in section 3b). Despite the similar intensity of the zonal-mean surface forcing in the NAMERICA and ASIA experiments (see Fig. 1c), the global response to the Atlantic LSC, consisting of a deepening of the geopotential height field over the North Atlantic sector and at high latitudes (Fig. 3f), is at least 50% weaker. On top of this, we see that, apart from a few regional exceptions, the response to TOTAL is approximately linear with respect to the responses to NAMERICA and ASIA forcings (cf. Fig. S2 and Fig. 3).

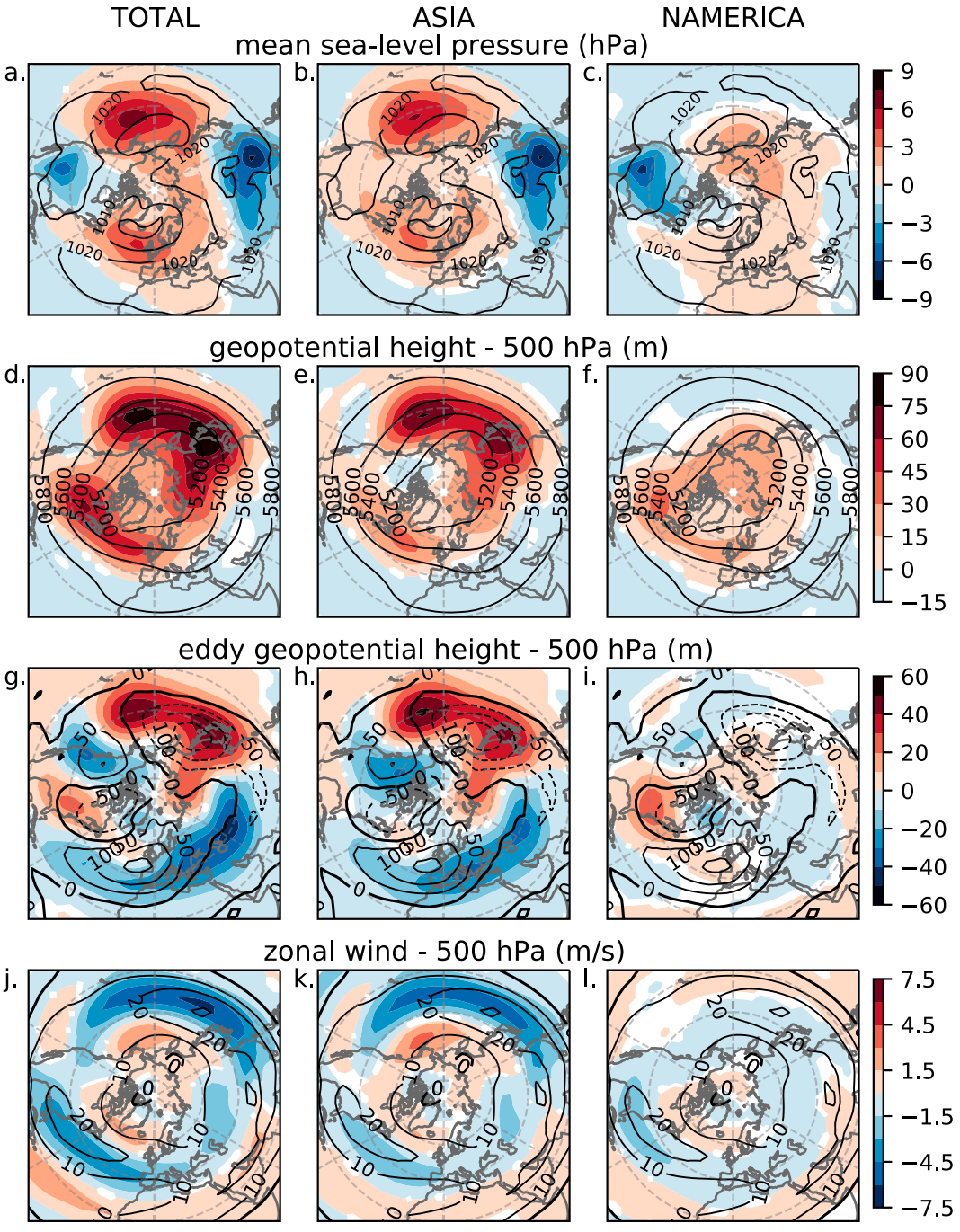

FIG. 3. The response of TOTAL, ASIA, and NAMERICA (shading) with respect to the CONTROL climatology (contours) for (a)–(c) mean sea level pressure, (d)–(f) geopotential height at 500 hPa and (g)–(i) its eddy component, and (j)–(l) zonal wind at 500 hPa. Shading indicates significant anomalies at a 95% confidence level according to a permutation test repeated 1000 times (Wilks 2011).

Large stationary waves (wave 1 and 2 in particular) are mainly attributable to extratropical thermal contrasts and orographic forcing (Held 1983; Held and Ting 1990), with the position of wave 1 related to the large-scale and high-amplitude signal generated by the Eurasian continent (cf. Figs. 4a and 4b, showing the first two zonal wavenumbers of the surface and midtroposphere CONTROL climatology, with the contours in Figs. 3a and 3g, comprehensive of all wavenumbers). While

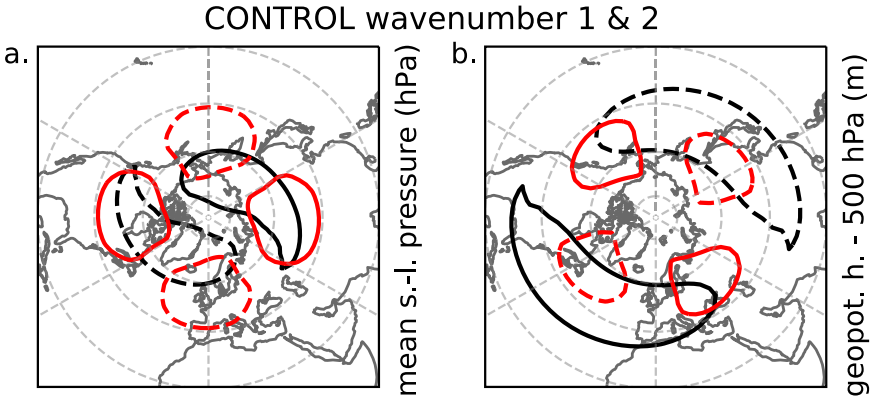

FIG. 4. Decomposition of the CONTROL climatology in zonal wavenumber 1 (black) and 2 (red) for (a) mean sea level pressure with contours at ±4 hPa and (b) 500-hPa geopotential height with contours at ±40 m.

ASIA forcing induces a weakening of stationary wave 1 (by ~30% at the surface and ~5% in the midtroposphere[3]) and wave 2 (by ~20% at the surface and in the midtroposphere), the NAMERICA response consists in a wave-2 attenuation (by ~15% at the surface and ~5% in the midtroposphere) and wave-1 amplification near the surface (by ~30% stronger; cf. the positive anomaly over Siberia and the North Pacific in Fig. 3c and the positive lobe of wave 1 in Fig. 4a). A general feature, particularly noticeable in experiment NAMERICA, is that the influence of the surface forcing on waves 1 and 2 is less evident in the midtroposphere (cf. Figs. 3 and 4).

A focus on the meridional cross sections of the atmosphere shows a different warming pattern when comparing experiment ASIA, where the positive temperature anomaly is confined to the midtroposphere and hardly reaches latitudes above 70°N, to experiment NAMERICA, showing a positive anomaly that extends to most of the high-latitude atmospheric column up to the stratosphere (see air temperature in the Atlantic and Pacific sectors; shading in Fig. 5). The northward extension of the lower-troposphere temperature anomalies in NAMERICA (Figs. 5d,h) is coherent with the amplification of MSLP wave 1 favoring the poleward heat transport through the North Atlantic sector (Graversen and Burtu 2016). The polar-cap heating decays in the midtroposphere, together with the amplification of wave 1, to become again relevant in the top levels. In the stratosphere the temperature profiles are linked to the dynamic response, as the westerly mean flow weakens with positive polar-latitude temperature anomalies and vice versa, following the thermal-wind relation.

To study the nearly opposite response of the midlatitude and polar stratosphere to the two individual-continent forcings (i.e., stratospheric cooling and vortex strengthening in ASIA; also applicable to TOTAL) and the opposite conditions in NAMERICA, we compute the vertical component of the Eliassen–Palm flux (E-P flux). The vertical E-P flux is proportional to the meridional eddy heat flux [Eq. (1)] and represents the vertical wave propagation (arrows in Fig. 6a). Since the convergence of the E-P flux in the stratospheric levels corresponds to a deposition of easterly momentum into the westerly mean flow (negative shading above 200 hPa at 40°–70°N in Fig. 6a), we expect an enhanced upper-level convergence to be associated to a weak stratospheric vortex and a warm polar stratosphere, the opposite for reduced stratospheric convergence. As a caveat, the small number of stratospheric levels in SPEEDY (see appendix A) limits the sensitivity of the EP-flux convergence diagnosis.

For ASIA and TOTAL experiments we find a net reduction of the meridional eddy heat flux into the stratosphere (Figs. 6b,c) at ~40°–60°N, the latitudes corresponding to the strongest climatological upward propagation (Fig. 6a). Note that this type of signal resembles that of strong stratospheric-vortex events (Fig. 4f in Díaz-Durán et al. 2017) and, indeed, in the topmost model level we find a weakening of the E-P flux convergence associated with an acceleration of the zonal-mean zonal wind. In the NAMERICA simulations a weak convergence anomaly in the stratospheric E-P flux and a vortex deceleration are detected (Fig. 6d). To better understand the mechanism leading to vortex weakening in NAMERICA we plot zonal wavenumbers 1 and 2 of the vertical E-P flux (Fig. S3), as these are known to dominate the wave propagation from the troposphere to the stratosphere (Charney and Drazin 1961; Andrews et al. 1987; Haklander et al. 2007). It is thus evident from Figs. S3d, S3h, and S3l that the slowing down of the stratospheric vortex in NAMERICA is caused by a moderate amplification of wave-1 E-P flux into the stratosphere; the reduction of the wave-2 component in the lower troposphere hardly reaches stratospheric levels. Differently, for ASIA the wave-1 and wave-2 components of the E-P flux are reduced (Figs. S3g,k), but again it is mainly the former that influences the strength of the stratospheric vortex.

In both the ASIA and NAMERICA experiments the low-wavenumber anomalies in the upward E-P flux originate in

[3] The estimate is computed by considering the ratio between the wave amplitude in ASIA or NAMERICA and that in the CONTROL, averaged over latitudes 40°–70°N. We use the fields of MSLP (surface) and of 500-hPa geopotential height (midtroposphere).

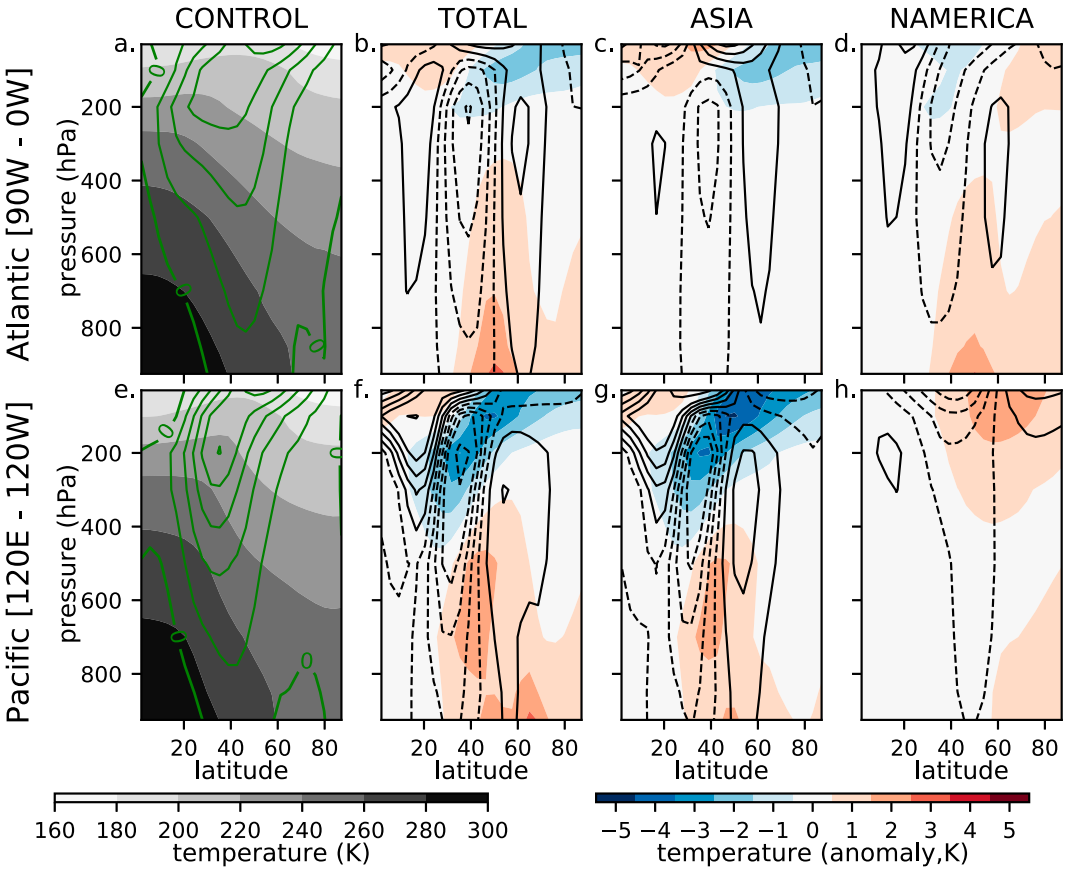

FIG. 5. Meridional cross sections of temperature (shading) and zonal wind (contours) in the (top) Atlantic sector and (bottom) Pacific sector; the response of (b),(f) TOTAL, (c),(g) ASIA, and (d),(h) NAMERICA is shown with respect to the (a),(e) CONTROL climatology. Contours are drawn every 10 m s^{-1} in (a) and (e), and every 1.2 m s^{-1} in (b)–(d) and (f)–(h).

the lower troposphere and decay in the midtroposphere, but nonetheless reach the topmost atmospheric layers. This is in agreement with the previous analysis on waves 1 and 2 at the surface (MSLP field) and in the midtroposphere (500-hPa geopotential height field).

The change in the wave activity propagating into the stratosphere is also detected in the v^*T^* anomaly at 200 hPa. In TOTAL and ASIA (Figs. 7a,b) the three centers of strongest positive v^*T^* (central Siberia, North Pacific, and western North Atlantic) are weaker by ~50% due to the reduction in the eddy components of the temperature field and to the weakening of the meridional circulation (discussed in section 3b). Differently, in NAMERICA the v^*T^* centers over the North Pacific (positive) and over North America (negative) are moderately amplified, while the positive v^*T^* over the North Atlantic–European region weakens over the ocean and strengthens over the continent. Since the meridional circulation is nearly unchanged, such signal is dominated by the changes in the eddy temperature pattern.

b. *Midlatitude jets*

The general response to the reduction of extratropical LSC consists in a weakening and poleward shift of the midlatitude jets. Specifically, the zonal winds weaken south of 50°N (Fig. 3j) following the reduction of the meridional gradients in the midtroposphere at ~30°–50°N (Fig. 3d), while they strengthen along the northern flanks of the jets (~50°–70°N) associated with reinforced meridional gradients (cf. Figs. 3d and 3j). The signal is coherent in the vertical up to ~200 hPa (Fig. 5); once more it is evident that the ASIA response, extending to the Atlantic sector, has a large influence on the midlatitude zonal flow (Fig. 5c).

The question might arise whether the modifications in the zonal flow are an effect of the LSC reduction or if they constitute a response to the generalized extratropical warming introduced by the forcing. To investigate this, we devise a new experiment, called ZMEAN-TOTAL, where the zonal-mean forcing from TOTAL is retained and spread uniformly over sea and land surface[4] (Fig. 8a). Such configuration produces a zonal-mean forcing equal to that in experiment TOTAL in spite of a zonal LSC similar to that in the CONTROL. The results indicate that the Pacific LSC is relevant for the

[4] We impose 2 times the zonal-mean ASIA forcing in the sector 60°–240°E, and 2 times the zonal-mean NAMERICA forcing in the sector 120°W–60°E.

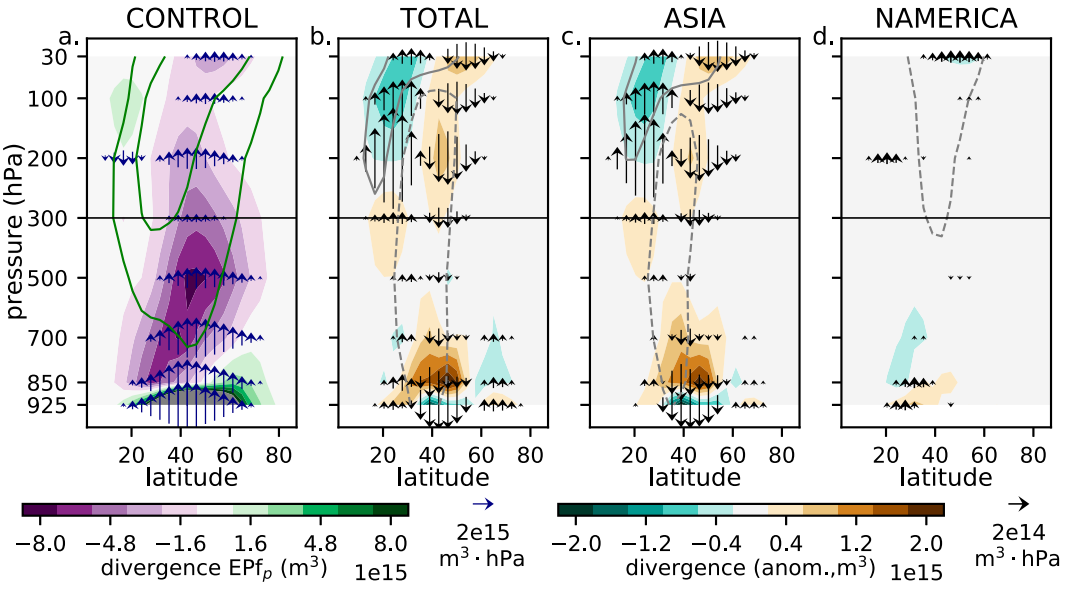

FIG. 6. Meridional cross sections of the vertical Eliassen–Palm flux (arrows) and its divergence (shading) for (a) CONTROL climatology, (b) TOTAL, (c) ASIA, and (d) NAMERICA anomalies. E-P fluxes above the 300-hPa horizontal line are multiplied by a factor of 5. Green contours in (a) show the zonal-mean zonal wind at 10 and 30 m s^{-1} levels; gray contours in (b)–(d) indicate the anomaly of each experiment for levels ± 1 m s^{-1}.

atmospheric circulation, independently of the generalized warming generated by the forcing. In fact, while in TOTAL the reduction of the Atlantic jet is to a certain extent similar to that in ZMEAN-TOTAL, suggesting a significant role of the generalized meridional temperature gradient, the TOTAL and ZMEAN-TOTAL Pacific-jet responses are different in position and intensity (cf. Figs. 3j and 8b).

The response to ASIA forcing is strong also in the Atlantic sector, where the damping of the Rockies' wave train crossing North America reduces the western ridge and eastern trough. This orographic wave is decisive for the localization of the Atlantic storm track along the southeastern coast of North America (i.e., where the baroclinicity is strongest; Brayshaw et al. 2009; Chang 2009). The attenuation of the Rockies' wave train (see the stationary eddy component of the geopotential height field in Fig. 3h and meridional wind field in Fig. 9a) is caused by the weakening of the lower-troposphere Pacific jet impinging on the Rocky Mountains (Held and Ting 1990; Held et al. 2002), with a pattern such as the one in Fig. 3k. The response to the altered orographic wave consists in a more zonal circulation in the North American region, with a weakened meridional wind over the eastern North Pacific and over the continent (Fig. 9a) and a positive zonal-wind anomaly at latitudes higher than 50°N (Fig. 3h). West of the Rockies the limited northward advection of warm air results in colder temperatures, while, in the area comprising the Hudson Bay, the diminished advection from the Arctic implies a warming over the eastern coast of North America (Fig. 9b) and a reduction in the baroclinicity at the entrance of the Atlantic storm track, as shown in section 3b.

The modification of the meridional circulation also affects the propagation of synoptic-eddy total energy flux (TEF) downstream of the Pacific (cf. Figs. 10b and 9a), which is known to play a role in setting the strength and position of the Atlantic jet (Chang 1993; James and Burkhardt 2006; Rivière and Orlanski 2007; Li and Lau 2012). Specifically, the

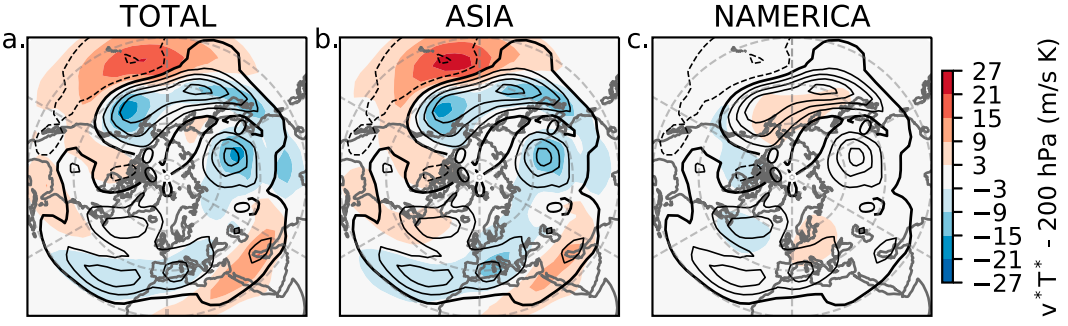

FIG. 7. The v^*T^* at 200 hPa, in shading the response of (a) TOTAL, (b) ASIA, and (c) NAMERICA with respect to the CONTROL climatology (contours every 10 m s^{-1} K).

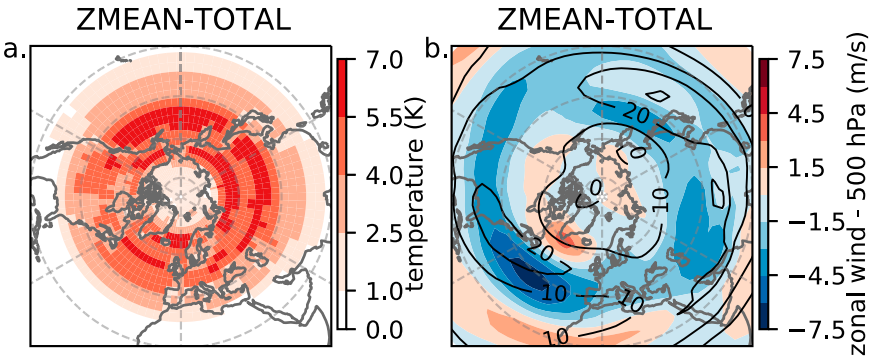

FIG. 8. (a) ZMEAN-TOTAL forcing anomaly averaged over January and February and (b) response of the zonal wind at 500 hPa (shading) with respect to the CONTROL climatology (contours).

upper-troposphere TEF is enhanced over the northern part of the Pacific basin and is advected zonally across the American continent, feeding the northward flank of the Atlantic storm track (Fig. 10b). The excess eddy energy does not reach southeastern North America, a key region for low-level cyclogenesis, characterized by a negative TEF anomaly induced by the weakening of the southward advection downstream of the Rockies (Fig. 9a) and by the reduction of the Pacific TEF south of 40°N and of its eastward propagation (Fig. 10b). The decline in synoptic upper-tropospheric disturbances over southeastern North America is thus expected to trigger less low-level cyclogenesis at the entrance of the Atlantic storm track [type-B cyclogenesis in Petterssen and Smebye (1971)].

In summary, in experiment ASIA the attenuation of the North American stationary wave weakens the baroclinicity over the eastern coast of the continent. This, together with less energetic upper-level disturbances entering the Atlantic domain south of 50°N, leads to a reduction in cyclogenesis and storm-track activity and, finally, to a reduction of the Atlantic jet (Fig. 3k).

c. *Storm tracks*

The tropospheric temperature anomalies induced by the surface forcings peak between 40° and 60°N and are accompanied by a weakening and poleward shift of the jets (Figs. 3j,l and 5b,f). These changes are associated with modifications in the synoptic variability, and in particular with poleward displaced midlatitude storm tracks (see shading, i.e., variance of high-frequency geopotential height, in Figs. 11b,f). ASIA forcing produces a strong, poleward shifted storm track over the Pacific, and a weakened and poleward shifted Atlantic storm track, which are in agreement with the low-level changes in baroclinicity expressed by the maximum Eady growth rate σ_{BI} (Figs. 11c,g). Moreover, a weakening of the Pacific storm track on its southeastern flank is balanced by a positive signal along the North Asian coast (not shown), giving no net storm-track decrease in the Pacific-sector zonal mean (Fig. 11g). For NAMERICA forcing we find weaker anomalies indicating a poleward shift of the storm track in the Atlantic sector (Fig. 11d) and a reduction of the storm track and of the jet over the Pacific basin, north of their maximum climatological intensity (Figs. 5h and 11h). Such negative signal in the Pacific storm track is difficult to justify exclusively by the corresponding moderate decrease in tropospheric baroclinicity (σ_{BI} contours in Fig. 11h).

Further reasoning for the storm-track and jet weakening could come from the effect of the lower stratosphere on the tropospheric mean state and variability. To give a simplistic picture, the weakening of the stratospheric vortex is known to cause a southward shift of the midlatitude tropospheric jets, while the opposite happens with a strong stratospheric vortex (Kidston et al. 2015); although regional differences might emerge between the Atlantic and Pacific basins, this behavior has been detected in models and in reanalysis (e.g., Polvani and Kushner 2002; Baldwin and Dunkerton 1999). The mechanisms for the downward propagation of stratospheric anomalies to the midlatitude troposphere are still debated. Despite a few exceptions (e.g., Smy and Scott 2009), models characterized by different levels of complexity show that an increase in lower-stratospheric shear tends to amplify the size and strength of baroclinic waves and to favor a northward displacement of the associated jet (see Wittman et al. 2007; Rivière 2011; Haualand and Spengler 2021; Rupp and Birner 2021; Butler et al. 2010).

Returning to the simulations, we note that in the CONTROL at latitudes up to 40°N the vertical wind shear near the tropopause (~200 hPa) is negative, with $(du/dz)_{\mathrm{str}} < 0 < (du/dz)_{\mathrm{tr}}$, while at higher latitudes it turns positive and it exceeds $(du/dz)_{\mathrm{tr}}$ (Figs. S4a,e), reproducing approximately the patterns of wind shear from reanalysis data (not shown). Following the arguments above, we hypothesize that in experiment NAMERICA the negative anomaly of the Pacific-sector lower-stratosphere wind shear (Fig. S4h), combined with the reduction in the tropospheric baroclinicity (contours in Fig. 11h), explains the weakening of the Pacific storm track (shading in Fig. 11h). In addition, the responses of the Atlantic and Pacific sectors to ASIA forcing may be supported by an analogous opposite influence of the upper-level wind shear on the tropospheric storm tracks. The increase in stratospheric zonal wind (Fig. 5c) and in its vertical shear (Fig. S4c) are indeed expected to favor the poleward shift detected in the NH jets and storm tracks (Figs. 5c and 11c).

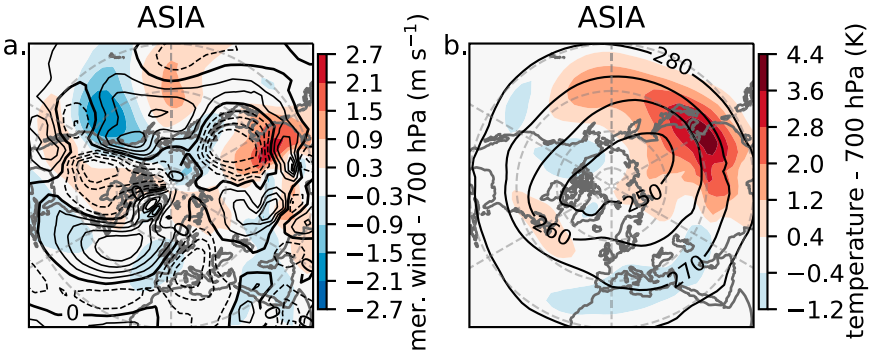

FIG. 9. (a) Meridional wind and (b) temperature at 700 hPa, showing the response of ASIA (shading) with respect to the CONTROL climatology (contours). In (a) contours are drawn every 1 m s^{-1}.

4. Discussion and conclusions

The reduction of midlatitude thermal land–sea contrast (LSC) is a robust characteristic of long-term climate projections (Table 1), with a negative trend already detectable in reanalysis data: ERA5 shows a weakening of LSC_{Pac} and LSC_{Atl} by 1.2 K (±1.0 K) between 1979 and 2020. Here, by running idealized numerical experiments where we impose surface warming over NH continents and climatological SSTs, we find that the response to a reduced boreal LSC consists in a reduction of the tropospheric stationary eddies propagating up to the stratosphere (Figs. 3g and 6b), and in a weakening and poleward shift of the midlatitude jets and of the associated storm tracks (Figs. 3j and 11b,f). This is in line with previous literature on the topic (Brayshaw et al. 2009; Held et al. 2002; Garfinkel et al. 2020) and shows the tendency of the mean NH regime to shift toward a more zonal circulation for a weaker zonal asymmetry in the surface thermal structure (thermal equilibration theory; see, e.g., Charney and DeVore 1979). In our study for the first time a distinction between the Pacific and Atlantic LSC is applied to disentangle their impact on the midlatitude atmosphere; note that the responses to individual East Asian and North American surface forcings add almost linearly to give the response to the sum of the forcings (Fig. 3 and Fig. S2).

If over North America the stationary waves are mainly attributable to the presence of the Rockies interacting with the low-level mean flow, the Siberian surface-pressure high forms in winter due to both the Tibetan Plateau orographic wave (Held 1983; Held et al. 2002) and the vast extent of Eurasia impeding warm-air advection from the oceanic regions (Seager et al. 2002). The large-scale patterns associated with the Siberian high/Aleutian low in the Pacific sector and eastern American high/Icelandic low in the Atlantic sector are reinforced by the atmospheric response to the strong ocean-to-atmosphere heat flux in the western portion of the NH oceans (i.e., a surface upstream high and a downstream low; Kaspi and Schneider 2011). These circulation systems imply a northerly advection of cold continental air over the western oceans which increases the air–sea temperature difference and enhances the heat flux from the ocean, hence inducing a positive feedback on the circulation. Our results suggest that a reduction of the LSC, Atlantic or Pacific, is consistent with a weakening of the eastern continents' highs and oceanic lows (Figs. 3a–c) induced by a decline in the heating effect by the warm western boundary oceanic currents (see Fig. S1 in the online supplemental material; Held et al. 2002; Kaspi and Schneider 2011) and by the weakening of the midlatitude jets (Fig. 3j).

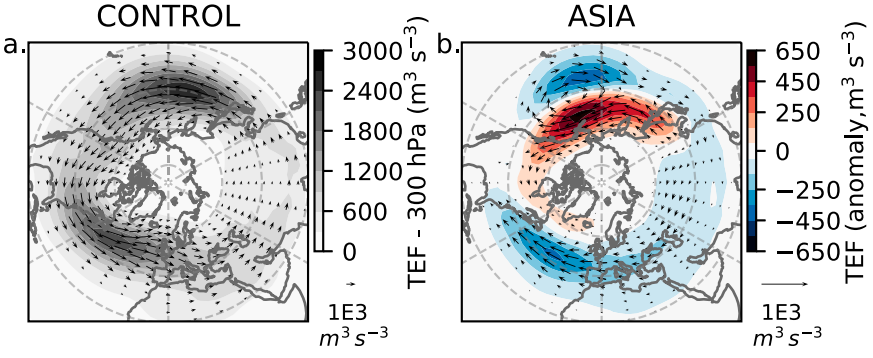

FIG. 10. Eddy total energy flux at 300 hPa (arrows) and its intensity (shading) for (a) the CONTROL climatology and (b) ASIA anomalies; in (b) the size of the arrows is amplified by a factor of 5.

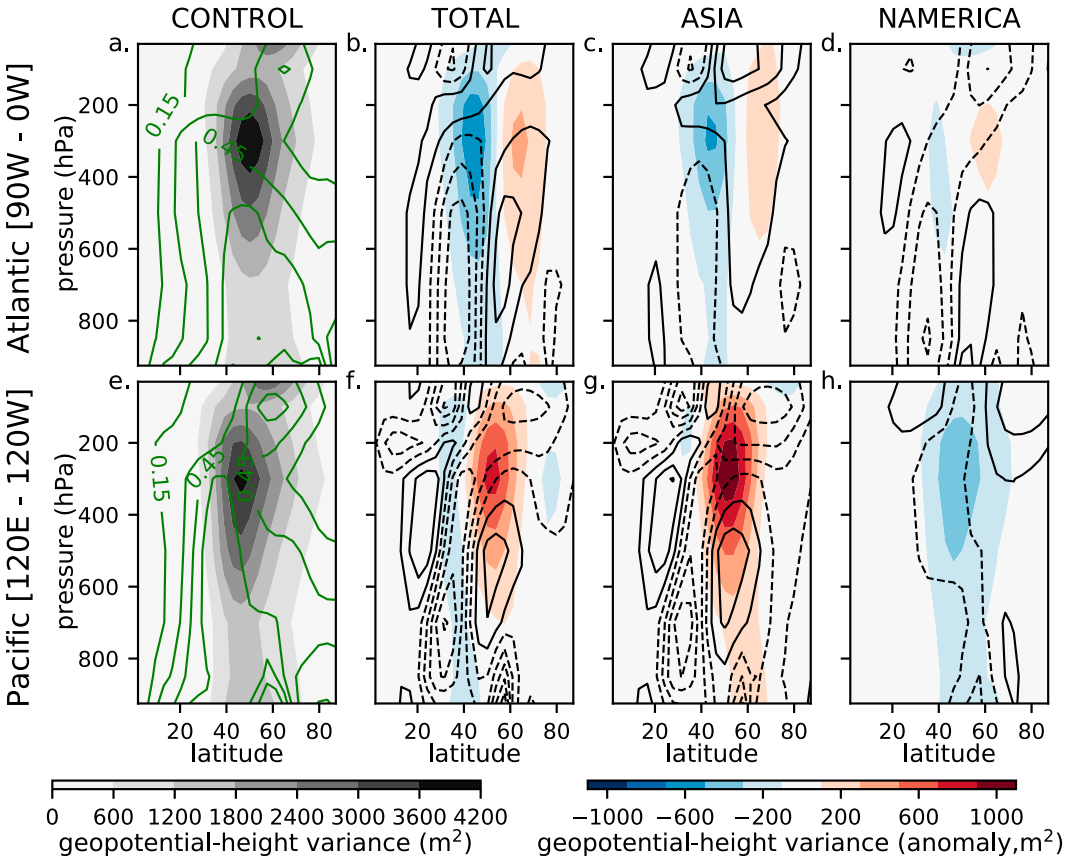

FIG. 11. Meridional cross sections of high-frequency geopotential height variance (shading) and maximum Eady growth rate (contours) in the (top) Atlantic sector and (bottom) Pacific sector. The responses of (b),(f) TOTAL, (c),(g) ASIA, and (d),(h) NAMERICA are shown with respect to the CONTROL climatology in (a) and (e). Contours are drawn every 0.15 day^{-1} in (a) and (e), and every 0.02 day^{-1} in (b)–(d) and (f)–(h).

Our idealized experiments show a dominant impact of East Asian surface temperatures on stationary planetary waves. Indeed the response to Asian warming interferes destructively with waves 1 and 2 (cf. Figs. 3 and 4) and reduces the propagation of large waves to the stratosphere, making the stratospheric vortex stronger (Fig. 6c). Hence, we confirm the sensitivity of the NH atmospheric circulation to the Pacific-sector surface conditions, as in Ayarzagüena et al. (2021), who attest to an important impact of the Pacific-sector SST on atmospheric planetary waves up to the stratosphere, or as in Cohen et al. (2014), linking anomalous Siberian snow cover to a weakened stratospheric vortex (this is consistent with the strong vortex in the warm-Asia experiment). The role of Eurasia for the vertical propagation of waves into the stratosphere is important also in model predictions (e.g., Domeisen et al. 2020; Portal et al. 2022). The relevance of the Pacific LSC, as opposed to a generalized midlatitude warming, is proved by the fact that a widespread reduction of the meridional surface-temperature gradients in the Pacific sector (Fig. 8) does not reproduce the position and intensity of the Pacific jet weakening obtained by warming East Asia (Fig. 3k). Downstream effects of the weakening of the Pacific jet consist of an attenuation of the Rockies' orographic wave and of the baroclinicity and cyclogenesis in the Atlantic jet-entry region (Figs. 9–11), and hence a slower and poleward displaced Atlantic jet (Fig. 5c).

The impact of reduced Atlantic LSC is less evident in the midtroposphere and seems to reach remote tropospheric regions mainly through a stratospheric pathway. We note an enhancement in wave-1 vertical propagation that leads to a warming of the stratosphere, a weakening of the vortex (Fig. 6d), and a reduction of the lower-stratospheric wind shear over the Pacific sector. We hypothesize that the latter is responsible for the negative anomaly in the Pacific storm track and jet (Figs. 11h and 5h). Despite the fact that our results highlight the importance of thermal changes over the midlatitude Pacific sector, long-term climate projections predict an enhanced reduction of the Atlantic LSC with respect to the Pacific LSC (Table 1). Understanding whether the effects of a reduced Atlantic LSC—including the weakening of the stratospheric vortex—would dominate in the projected configuration of LSC is beyond the scope of this paper.

We indicate some possible shortcomings in this work. First, the surface temperature over the sea is fixed and that over land is relaxed toward the LST forcing patterns. This restricts the two-way interaction between the surface and the atmosphere

(see appendix B) and removes the interdependence between the SSTs and the land temperature. While the arrangement is satisfactory for the analysis of a long-term LSC change of amplitude larger than its interannual variations, additional work is necessary to assess whether our results are also relevant for the impact of LSC on year-to-year variability.

A further limitation derives from the coarse resolution of the model. Kucharski et al. (2013) and the articles there cited show that the model SPEEDY reliably represents the large-scale features of the climate mean and variability in the midlatitudes. According to more recent papers (Ruggieri et al. 2017; Hamouda et al. 2021) the limited representation of the stratospheric system does not inhibit the coupling between the troposphere and the stratosphere (see appendix A for an exhaustive discussion). Furthermore, the bias in the representation of the model orography, dependent on the horizontal resolution, may influence the model response.

Our results describe the role played by decreasing LSC in the midlatitude mean climate and variability. In CMIP6 scenarios the larger land temperature increase in the NH middle and high latitudes than elsewhere reduces the extratropical LSC by various degrees, with an amplitude comparable to that of Arctic amplification (AA) (IPCC 2021). However, differently from AA, LSC is rarely cited when analyzing the sources of the projected changes in the large-scale midlatitude circulation, such as those concerning stationary planetary waves (Wills et al. 2019, and references therein) and tropospheric jets and storm tracks (e.g., Harvey et al. 2020; Oudar et al. 2020; Shaw et al. 2016). Our results suggest that in the "tug of war" between the AA and the Hadley cell expansion for the positioning of the jet stream (Butler et al. 2010; Barnes and Polvani 2013), a reduced LSC supports the effects of the latter—a poleward jet shift. We therefore encourage research on climate change scenarios to take into account LSC as a possible source of change for the midlatitude circulation and to investigate its interplay with AA.

Acknowledgments. The authors are thankful to Franco Molteni for insightful discussion and advice. This work is an outcome of Project MIUR "Dipartimenti di Eccellenza 2018-2022". C.P. gratefully acknowledges hospitality and support from the Department of Geosciences, École Normale Supérieure, during part of this work.

Data availability statement. Additional information on ICTP AGCM "SPEEDY" is available at the following link: https://www.ictp.it/research/esp/models/speedy.aspx. The ERA5 and HadISST reanalyses and the CMIP5 dataset are publicly available.

APPENDIX A

Stratospheric Levels in SPEEDY

The stratosphere in SPEEDY consists of two atmospheric levels at 100 and 30 hPa. In the top level (30 hPa) a drag on the zonal-mean winds with relaxation time of 1 month is implemented to obtain a climatology close to the observed one; this level also acts as a "sponge layer" thanks to additional diffusion with a relaxation time of 12 h. The model is not equipped with an atmospheric chemistry scheme; hence the absorption of radiation in the stratosphere is prescribed by a zonally symmetric function with a suitable seasonal cycle. Thus, the top two levels of the model provide a "bulk" representation of the stratosphere, which serve as boundary conditions for reproducing the effects of the stratosphere on the troposphere (King et al. 2010). As reported in King et al. (2010), Herceg-Bulić et al. (2017), and Ruggieri et al. (2017), the stratospheric variability and troposphere–stratosphere coupling are remarkably well represented in SPEEDY considering the scarcity of stratospheric levels, and are comparable with results from higher-complexity and finer-resolution atmospheric models [see Fig. 11 in King et al. (2010)]; however, the vertical coupling develops faster in SPEEDY than in finer-resolved models and in reanalysis (Herceg-Bulić et al. 2017).

APPENDIX B

Land-Temperature and Ice-Temperature Schemes

The skin temperature over land (T_{skin}), computed separately from the land surface temperature (LST, i.e., the temperature in the upper layer of soil), follows the equation of energy balance at the surface:

$$k_l(T_{\text{skin}} - \text{LST}) = F^{\text{SR}} + F^{\text{LR}} + \text{SHF}_l + \text{LHF}_l = \text{GHS}_l, \tag{B1}$$

where the ground heat flux on land (GHS_l) is the sum over shortwave and longwave radiation fluxes (F^{SR}, F^{LR}), sensible heat flux over land (SHF_l), and latent heat of evaporation over land (LHF_l), all computed assuming $T_{\text{skin}} = \text{LST}$; k_l is the coefficient for land heat flux. Further details on the solution of Eq. (B1) and on the form of the different heat-flux components can be found in Molteni and Kucharski (2016). The LST adjusts to the incoming heat flux and, at the same time, relaxes toward a prescribed monthly seasonal cycle LST_{cl}, as in

$$d_s\, c_s \frac{\partial \text{LST}}{\partial t} = \text{GHS}_l - d_s\, c_s\, \tau_s^{-1}(\text{LST} - \text{LST}_{\text{cl}}), \tag{B2}$$

where d_s is the depth of the interactive soil layer (1 m), c_s is the heat capacity of the soil, and τ_s is the damping time scale for soil temperature anomalies (40 days). When the land-temperature scheme in Eq. (B2) is deactivated then LST is fixed to its climatological value.

The model includes a scheme for sea ice temperature (SIT) analog to that of land surface temperature

$$d_i\, c_i \frac{\partial \text{SIT}}{\partial t} = \text{GHS}_s - d_i\, c_i\, \tau_i^{-1}(\text{SIT} - \text{SIT}_{\text{cl}}), \tag{B3}$$

characterized by GHS_s (the ground heat flux on the sea, computed using the SST), c_i (the heat capacity of sea ice), a depth varying according to $d_i = d_M + (d_m - d_M)\cos(\phi)^2$

(d_M = 2.5 m, d_m = 1.5 m, ϕ being the latitude), and a damping time scale τ_i of 30 days. The anomaly of SIT from its climatology adjusts to the incoming heat flux, while the SIC is always fixed to its prescribed climatology. As in the case of the land surface temperature, SIT corresponds to its climatological value (SIT_{cl}) when the sea ice scheme is suppressed.

Despite the sea surface temperature being prescribed in all experiments, when the sea ice scheme is activated the SST may deviate from its prescribed climatology (SST_{cl}) by the quantity $(SIT - SIT_{cl}) \times SIC_{cl}$, where SIT and SIT_{cl} are the sea ice temperature and its climatology, and SIC_{cl} is the climatological sea ice concentration. Moreover, SST_{cl} corresponds to the grid box average over the climatological values of liquid water temperature (ST_{cl}) and SIT_{cl}, weighted by their respective concentrations ($1 - SIC_{cl}$ and SIC_{cl}). Whereas SST_{cl} and SIC_{cl} are provided as an input, ST_{cl} and SIT_{cl} are computed directly by the model by fixing SIT_{cl} (ST_{cl}) to 271.4 K, seawater freezing temperature, when SST_{cl} is above (below) freezing. Moreover, the minimum SIC_{cl} is 0.1 when SST_{cl} is below freezing.

APPENDIX C

Forcing Patterns

The pattern of LST forcing shown in Fig. 1b is computed from a mean between the January/February and the April LST_{mod}

$$LST_{TOT}(m, C) = \frac{LST_{mod}(m, C) + \mathscr{A}(C)\sin(\phi)LST_{mod}(\text{Apr}, C)}{1 + \mathscr{A}(C)\sin(\phi)}, \tag{C1}$$

where m indicates the month (January or February), $\mathscr{A}(C)$ is a coefficient depending on the continent C ($\mathscr{A}$ is set to 8 for C = North America and to 4 for C = Asia), and the weight of the April LST grows with the sine of the latitude ϕ. This is done to obtain a large midlatitude LST forcing that becomes unimportant in the tropics. In addition, the anomaly $\Delta LST_{TOT} = LST_{TOT} - LST_{mod}$ is multiplied by a factor of 1.5 over North America. Both the amplification factor and the coefficient $\mathscr{A}$ are modulated to obtain zonal-mean forcing and LSC reduction of similar intensity over the two continents so as to compare experiments ASIA and NAMERICA (run with the individual continental anomalies from Fig. 1b). We note that the April LST is chosen against summer LST because its temperature pattern is reflective of a dynamics that is reminiscent of the winter one (e.g., in terms of stationary planetary waves; Wang and Ting 1999); moreover, the latitudinal profile of the forcing pattern (weighted by the sine of latitude) recalls that of NH land surface warming in scenarios of the future climate (IPCC 2021).

REFERENCES

Andrews, D. G., J. R. Holton, and C. B. Leovy, 1987: *Middle Atmosphere Dynamics.* Academic Press, 40 pp.

Ayarzagüena, B., E. Manzini, N. Calvo, and D. Matei, 2021: Interaction between decadal-to-multidecadal oceanic variability and sudden stratospheric warmings. *Ann. N. Y. Acad. Sci.*, **1504**, 215–229, https://doi.org/10.1111/nyas.14663.

Baldwin, M. P., and T. J. Dunkerton, 1999: Propagation of the Arctic oscillation from the stratosphere to the troposphere. *J. Geophys. Res.*, **104**, 30 937–30 946, https://doi.org/10.1029/1999JD900445.

Barnes, E. A., and L. Polvani, 2013: Response of the midlatitude jets, and of their variability, to increased greenhouse gases in the CMIP5 models. *J. Climate*, **26**, 7117–7135, https://doi.org/10.1175/JCLI-D-12-00536.1.

Blackport, R., and J. A. Screen, 2020: Insignificant effect of Arctic amplification on the amplitude of midlatitude atmospheric waves. *Sci. Adv.*, **6**, eaay2880, https://doi.org/10.1126/sciadv.aay2880.

Brayshaw, D. J., B. Hoskins, and M. Blackburn, 2009: The basic ingredients of the North Atlantic storm track. Part I: Land–sea contrast and orography. *J. Atmos. Sci.*, **66**, 2539–2558, https://doi.org/10.1175/2009JAS3078.1.

Butler, A. H., D. W. Thompson, and R. Heikes, 2010: The steady-state atmospheric circulation response to climate change–like thermal forcings in a simple general circulation model. *J. Climate*, **23**, 3474–3496, https://doi.org/10.1175/2010JCLI3228.1.

Chang, E. K., 1993: Downstream development of baroclinic waves as inferred from regression analysis. *J. Atmos. Sci.*, **50**, 2038–2053, https://doi.org/10.1175/1520-0469(1993)050<2038:DDOBWA>2.0.CO;2.

——, 2009: Diabatic and orographic forcing of northern winter stationary waves and storm tracks. *J. Climate*, **22**, 670–688, https://doi.org/10.1175/2008JCLI2403.1.

Charney, J. G., and P. G. Drazin, 1961: Propagation of planetary-scale disturbances from the lower into the upper atmosphere. *J. Geophys. Res.*, **66**, 83–109, https://doi.org/10.1029/JZ066i001p00083.

——, and J. G. DeVore, 1979: Multiple flow equilibria in the atmosphere and blocking. *J. Atmos. Sci.*, **36**, 1205–1216, https://doi.org/10.1175/1520-0469(1979)036<1205:MFEITA>2.0.CO;2.

Cohen, J., K. Saito, and D. Entekhabi, 2001: The role of the Siberian high in Northern Hemisphere climate variability. *Geophys. Res. Lett.*, **28**, 299–302, https://doi.org/10.1029/2000GL011927.

——, J. C. Furtado, J. Jones, M. Barlow, D. Whittleston, and D. Entekhabi, 2014: Linking Siberian snow cover to precursors of stratospheric variability. *J. Climate*, **27**, 5422–5432, https://doi.org/10.1175/JCLI-D-13-00779.1.

——, and Coauthors, 2020: Divergent consensuses on Arctic amplification influence on midlatitude severe winter weather. *Nat. Climate Change*, **10**, 20–29, https://doi.org/10.1038/s41558-019-0662-y.

Day, J. J., and K. I. Hodges, 2018: Growing land–sea temperature contrast and the intensification of Arctic cyclones. *Geophys. Res. Lett.*, **45**, 3673–3681, https://doi.org/10.1029/2018GL077587.

de Vries, H., R. J. Haarsma, and W. Hazeleger, 2012: Western European cold spells in current and future climate. *Geophys. Res. Lett.*, **39**, L04706, https://doi.org/10.1029/2011GL050665.

Díaz-Durán, A., E. Serrano, B. Ayarzagüena, M. Abalos, and A. de la Cámara, 2017: Intra-seasonal variability of extreme boreal stratospheric polar vortex events and their precursors. *Climate Dyn.*, **49**, 3473–3491, https://doi.org/10.1007/s00382-017-3524-1.

Domeisen, D. I., and Coauthors, 2020: The role of the stratosphere in subseasonal to seasonal prediction: 2. Predictability

arising from stratosphere–troposphere coupling. *J. Geophys. Res. Atmos.*, **125**, e2019JD030923, https://doi.org/10.1029/2019JD030923.

Drijfhout, S., G. J. Van Oldenborgh, and A. Cimatoribus, 2012: Is a decline of AMOC causing the warming hole above the North Atlantic in observed and modeled warming patterns? *J. Climate*, **25**, 8373–8379, https://doi.org/10.1175/JCLI-D-12-00490.1.

Drouard, M., G. Rivière, and P. Arbogast, 2015: The link between the North Pacific climate variability and the North Atlantic oscillation via downstream propagation of synoptic waves. *J. Climate*, **28**, 3957–3976, https://doi.org/10.1175/JCLI-D-14-00552.1.

Garfinkel, C. I., I. White, E. P. Gerber, M. Jucker, and M. Erez, 2020: The building blocks of Northern Hemisphere wintertime stationary waves. *J. Climate*, **33**, 5611–5633, https://doi.org/10.1175/JCLI-D-19-0181.1.

Graversen, R. G., and M. Burtu, 2016: Arctic amplification enhanced by latent energy transport of atmospheric planetary waves. *Quart. J. Roy. Meteor. Soc.*, **142**, 2046–2054, https://doi.org/10.1002/qj.2802.

Gregory, J. M., and J. Mitchell, 1995: Simulation of daily variability of surface temperature and precipitation over Europe in the current and 2 × CO_2 climates using the UKMO climate model. *Quart. J. Roy. Meteor. Soc.*, **121**, 1451–1476, https://doi.org/10.1002/qj.49712152611.

Haklander, A., P. Siegmund, and H. Kelder, 2007: Interannual variability of the stratospheric wave driving during northern winter. *Atmos. Chem. Phys.*, **7**, 2575–2584, https://doi.org/10.5194/acp-7-2575-2007.

Hamouda, M. E., C. Pasquero, and E. Tziperman, 2021: Decoupling of the Arctic Oscillation and North Atlantic Oscillation in a warmer climate. *Nat. Climate Change*, **11**, 137–142, https://doi.org/10.1038/s41558-020-00966-8.

Harvey, B., P. Cook, L. Shaffrey, and R. Schiemann, 2020: The response of the Northern Hemisphere storm tracks and jet streams to climate change in the CMIP3, CMIP5, and CMIP6 climate models. *J. Geophys. Res. Atmos.*, **125**, e2020JD032701, https://doi.org/10.1029/2020JD032701.

Haualand, K. F., and T. Spengler, 2021: Relative importance of tropopause structure and diabatic heating for baroclinic instability. *Wea. Climate Dyn.*, **2**, 695–712, https://doi.org/10.5194/wcd-2021-13.

He, Y., J. Huang, and M. Ji, 2014: Impact of land–sea thermal contrast on interdecadal variation in circulation and blocking. *Climate Dyn.*, **43**, 3267–3279, https://doi.org/10.1007/s00382-014-2103-y.

——, ——, D. Li, Y. Xie, G. Zhang, Y. Qi, S. Wang, and S. Totz, 2018: Comparison of the effect of land–sea thermal contrast on interdecadal variations in winter and summer blockings. *Climate Dyn.*, **51**, 1275–1294, https://doi.org/10.1007/s00382-017-3954-9.

Held, I. M., 1983: Stationary and quasi-stationary eddies in the extratropical troposphere: Theory. *Large-Scale Dynamical Processes in the Atmosphere*, Academic Press, 127–168.

——, and M. Ting, 1990: Orographic versus thermal forcing of stationary waves: The importance of the mean low-level wind. *J. Atmos. Sci.*, **47**, 495–500, https://doi.org/10.1175/1520-0469(1990)047<0495:OVTFOS>2.0.CO;2.

——, ——, and H. Wang, 2002: Northern winter stationary waves: Theory and modeling. *J. Climate*, **15**, 2125–2144, https://doi.org/10.1175/1520-0442(2002)015<2125:NWSWTA>2.0.CO;2.

Herceg-Bulić, I., B. Mezzina, F. Kucharski, P. Ruggieri, and M. P. King, 2017: Wintertime ENSO influence on late spring European climate: The stratospheric response and the role of North Atlantic SST. *Int. J. Climatol.*, **37**, 87–108, https://doi.org/10.1002/joc.4980.

Hersbach, H., and Coauthors, 2020: The ERA5 global reanalysis. *Quart. J. Roy. Meteor. Soc.*, **146**, 1999–2049, https://doi.org/10.1002/qj.3803.

Hoskins, B. J., and P. J. Valdes, 1990: On the existence of storm-tracks. *J. Atmos. Sci.*, **47**, 1854–1864, https://doi.org/10.1175/1520-0469(1990)047<1854:OTEOST>2.0.CO;2.

IPCC, 2021: *Climate Change 2021: The Physical Science Basis.* Cambridge University Press, 3949 pp.

James, I. N., and U. Burkhardt, 2006: A sidelong look at storm tracks. *Atmos. Sci. Lett.*, **7**, 69–74, https://doi.org/10.1002/asl.134.

Kamae, Y., M. Watanabe, M. Kimoto, and H. Shiogama, 2014: Summertime land–sea thermal contrast and atmospheric circulation over East Asia in a warming climate—Part I: Past changes and future projections. *Climate Dyn.*, **43**, 2553–2568, https://doi.org/10.1007/s00382-014-2073-0.

Kaspi, Y., and T. Schneider, 2011: Winter cold of eastern continental boundaries induced by warm ocean waters. *Nature*, **471**, 621–624, https://doi.org/10.1038/nature09924.

Keil, P., T. Mauritsen, J. Jungclaus, C. Hedemann, D. Olonscheck, and R. Ghosh, 2020: Multiple drivers of the North Atlantic warming hole. *Nat. Climate Change*, **10**, 667–671, https://doi.org/10.1038/s41558-020-0819-8.

Kidston, J., A. A. Scaife, S. C. Hardiman, D. M. Mitchell, N. Butchart, M. P. Baldwin, and L. J. Gray, 2015: Stratospheric influence on tropospheric jet streams, storm tracks and surface weather. *Nat. Geosci.*, **8**, 433–440, https://doi.org/10.1038/ngeo2424.

King, M. P., F. Kucharski, and F. Molteni, 2010: The roles of external forcings and internal variabilities in the Northern Hemisphere atmospheric circulation change from the 1960s to the 1990s. *J. Climate*, **23**, 6200–6220, https://doi.org/10.1175/2010JCLI3239.1.

Kucharski, F., F. Molteni, and A. Bracco, 2006: Decadal interactions between the western tropical Pacific and the North Atlantic Oscillation. *Climate Dyn.*, **26**, 79–91, https://doi.org/10.1007/s00382-005-0085-5.

——, ——, M. P. King, R. Farneti, I.-S. Kang, and L. Feudale, 2013: On the need of intermediate complexity general circulation models: A "SPEEDY" example. *Bull. Amer. Meteor. Soc.*, **94**, 25–30, https://doi.org/10.1175/BAMS-D-11-00238.1.

Kushnir, Y., W. Robinson, I. Bladé, N. Hall, S. Peng, and R. Sutton, 2002: Atmospheric GCM response to extratropical SST anomalies: Synthesis and evaluation. *J. Climate*, **15**, 2233–2256, https://doi.org/10.1175/1520-0442(2002)015<2233:AGRTES>2.0.CO;2.

Labe, Z., Y. Peings, and G. Magnusdottir, 2020: Warm Arctic, cold Siberia pattern: Role of full Arctic amplification versus sea ice loss alone. *Geophys. Res. Lett.*, **47**, e2020GL088583, https://doi.org/10.1029/2020GL088583.

Li, Y., and N.-C. Lau, 2012: Impact of ENSO on the atmospheric variability over the North Atlantic in late winter—Role of transient eddies. *J. Climate*, **25**, 320–342, https://doi.org/10.1175/JCLI-D-11-00037.1.

Marshall, J., and D. W. So, 1990: Thermal equilibration of planetary waves. *J. Atmos. Sci.*, **47**, 963–978, https://doi.org/10.1175/1520-0469(1990)047<0963:TEOPW>2.0.CO;2.

Mitchell, H. L., and J. Derome, 1983: Blocking-like solutions of the potential vorticity equation: Their stability at equilibrium and growth at resonance. *J. Atmos. Sci.*, **40**, 2522–2536, https://doi.org/10.1175/1520-0469(1983)040<2522:BLSOTP>2.0.CO;2.

Molteni, F., 2003: Atmospheric simulations using a GCM with simplified physical parametrizations. I: Model climatology and variability in multi-decadal experiments. *Climate Dyn.*, **20**, 175–191, https://doi.org/10.1007/s00382-002-0268-2.

——, and F. Kucharski, 2016: Description of the ICTP AGCM (SPEEDY) version 40, Abdus Salam International Centre for Theoretical Physics, 17 pp., http://users.ictp.it/~kucharsk/speedy_description/km_ver40_appendixA.pdf.

——, M. P. King, F. Kucharski, and D. M. Straus, 2011: Planetary-scale variability in the northern winter and the impact of land–sea thermal contrast. *Climate Dyn.*, **37**, 151–170, https://doi.org/10.1007/s00382-010-0906-z.

Oudar, T., J. Cattiaux, and H. Douville, 2020: Drivers of the northern extratropical eddy-driven jet change in CMIP5 and CMIP6 models. *Geophys. Res. Lett.*, **47**, e2019GL086695, https://doi.org/10.1029/2019GL086695.

Petterssen, S., and S. Smebye, 1971: On the development of extratropical cyclones. *Quart. J. Roy. Meteor. Soc.*, **97**, 457–482, https://doi.org/10.1002/qj.49709741407.

Polvani, L. M., and P. J. Kushner, 2002: Tropospheric response to stratospheric perturbations in a relatively simple general circulation model. *Geophys. Res. Lett.*, **29**, 1114, https://doi.org/10.1029/2001GL014284.

Portal, A., P. Ruggieri, F. M. Palmeiro, J. García-Serrano, D. I. Domeisen, and S. Gualdi, 2022: Seasonal prediction of the boreal winter stratosphere. *Climate Dyn.*, **58**, 2109–2130, https://doi.org/10.1007/s00382-021-05787-9.

Previdi, M., K. L. Smith, and L. M. Polvani, 2021: Arctic amplification of climate change: A review of underlying mechanisms. *Environ. Res. Lett.*, **16**, 093003, https://doi.org/10.1088/1748-9326/ac1c29.

Rahmstorf, S., J. E. Box, G. Feulner, M. E. Mann, A. Robinson, S. Rutherford, and E. J. Schaffernicht, 2015: Exceptional twentieth-century slowdown in Atlantic Ocean overturning circulation. *Nat. Climate Change*, **5**, 475–480, https://doi.org/10.1038/nclimate2554.

Rayner, N., D. E. Parker, E. Horton, C. K. Folland, L. V. Alexander, D. Rowell, E. C. Kent, and A. Kaplan, 2003: Global analyses of sea surface temperature, sea ice, and night marine air temperature since the late nineteenth century. *J. Geophys. Res.*, **108**, 4407, https://doi.org/10.1029/2002JD002670.

Rivière, G., 2011: A dynamical interpretation of the poleward shift of the jet streams in global warming scenarios. *J. Atmos. Sci.*, **68**, 1253–1272, https://doi.org/10.1175/2011JAS3641.1.

——, and I. Orlanski, 2007: Characteristics of the Atlantic storm-track eddy activity and its relation with the North Atlantic Oscillation. *J. Atmos. Sci.*, **64**, 241–266, https://doi.org/10.1175/JAS3850.1.

Ruggieri, P., F. Kucharski, R. Buizza, and M. Ambaum, 2017: The transient atmospheric response to a reduction of sea-ice cover in the Barents and Kara Seas. *Quart. J. Roy. Meteor. Soc.*, **143**, 1632–1640, https://doi.org/10.1002/qj.3034.

Rupp, P., and T. Birner, 2021: Tropospheric eddy feedback to different stratospheric conditions in idealised baroclinic life cycles. *Wea. Climate Dyn.*, **2**, 111–128, https://doi.org/10.5194/wcd-2-111-2021.

Seager, R., D. S. Battisti, J. Yin, N. Gordon, N. Naik, A. C. Clement, and M. A. Cane, 2002: Is the Gulf Stream responsible for Europe's mild winters? *Quart. J. Roy. Meteor. Soc.*, **128**, 2563–2586, https://doi.org/10.1256/qj.01.128.

Serreze, M. C., and R. G. Barry, 2011: Processes and impacts of Arctic amplification: A research synthesis. *Global Planet. Change*, **77**, 85–96, https://doi.org/10.1016/j.gloplacha.2011.03.004.

Shaw, T., and A. Voigt, 2015: Tug of war on summertime circulation between radiative forcing and sea surface warming. *Nat. Geosci.*, **8**, 560–566, https://doi.org/10.1038/ngeo2449.

——, and Coauthors, 2016: Storm track processes and the opposing influences of climate change. *Nat. Geosci.*, **9**, 656–664, https://doi.org/10.1038/ngeo2783.

Smagorinsky, J., 1953: The dynamical influence of large-scale heat sources and sinks on the quasi-stationary mean motions of the atmosphere. *Quart. J. Roy. Meteor. Soc.*, **79**, 342–366, https://doi.org/10.1002/qj.49707934103.

Smy, L., and R. Scott, 2009: The influence of stratospheric potential vorticity on baroclinic instability. *Quart. J. Roy. Meteor. Soc.*, **135**, 1673–1683, https://doi.org/10.1002/qj.484.

Sutton, R. T., B. Dong, and J. M. Gregory, 2007: Land/sea warming ratio in response to climate change: IPCC AR4 model results and comparison with observations. *Geophys. Res. Lett.*, **34**, L02701, https://doi.org/10.1029/2006GL028164.

Taylor, K. E., R. J. Stouffer, and G. A. Meehl, 2012: An overview of CMIP5 and the experiment design. *Bull. Amer. Meteor. Soc.*, **93**, 485–498, https://doi.org/10.1175/BAMS-D-11-00094.1.

Valdes, P. J., and B. J. Hoskins, 1989: Linear stationary wave simulations of the time-mean climatological flow. *J. Atmos. Sci.*, **46**, 2509–2527, https://doi.org/10.1175/1520-0469(1989)046<2509:LSWSOT>2.0.CO;2.

Wallace, C., and M. Joshi, 2018: Comparison of land–ocean warming ratios in updated observed records and CMIP5 climate models. *Environ. Res. Lett.*, **13**, 114011, https://doi.org/10.1088/1748-9326/aae46f.

Wang, H., and M. Ting, 1999: Seasonal cycle of the climatological stationary waves in the NCEP–NCAR reanalysis. *J. Atmos. Sci.*, **56**, 3892–3919, https://doi.org/10.1175/1520-0469(1999)056<3892:SCOTCS>2.0.CO;2.

Wilks, D. S., 2011: *Statistical Methods in the Atmospheric Sciences.* Academic Press, 676 pp.

Wills, R. C., R. H. White, and X. J. Levine, 2019: Northern Hemisphere stationary waves in a changing climate. *Curr. Climate Change Rep.*, **5**, 372–389, https://doi.org/10.1007/s40641-019-00147-6.

Wittman, M. A., A. J. Charlton, and L. M. Polvani, 2007: The effect of lower stratospheric shear on baroclinic instability. *J. Atmos. Sci.*, **64**, 479–496, https://doi.org/10.1175/JAS3828.1.

Zhuang, M., A. Duan, R. Lu, P. Li, and J. Yao, 2022: Relative impacts of the orography and land–sea contrast over the Indochina peninsula on the Asian summer monsoon between early and late summer. *J. Climate*, **35**, 3037–3055, https://doi.org/10.1175/JCLI-D-21-0576.1.